Biotechnology for Biofuels and Bioproducts

RESEARCH

Open Access

Catalytic hydrolysis of agar using magnetic nanoparticles: optimization and characterization

Anoth Maharjan[1], Wonho Choi[2], Hee Taek Kim[3] and Jung-Ho Park[1,4*]

Abstract

Background Agar is used as a gelling agent that possesses a variety of biological properties; it consists of the polysaccharides agarose and porphyrin. In addition, the monomeric sugars generated after agar hydrolysis can be functionalized for use in biorefineries and biofuel production. The main objective of this study was to develop a sustainable agar hydrolysis process for bioethanol production using nanotechnology. Peroxidase-mimicking Fe_3O_4-MNPs were applied for agar degradation to generate agar hydrolysate-soluble fractions amenable to *Saccharomyces cerevisiae* and *Escherichia coli* during fermentation.

Results Fe_3O_4-MNP-treated (Fe_3O_4-MNPs, 1 g/L) agar exhibited 0.903 g/L of reducing sugar, which was 21-fold higher than that of the control (without Fe_3O_4-MNP-treated). Approximately 0.0181% and 0.0042% of ethanol from 1% of agar was achieved using *Saccharomyces cerevisiae* and *Escherichia coli*, respectively, after process optimization. Furthermore, different analytical techniques (FTIR, SEM, TEM, EDS, XRD, and TGA) were applied to validate the efficiency of Fe_3O_4-MNPs in agar degradation.

Conclusions To the best of our knowledge, Fe_3O_4-MNP-treated agar degradation for bioethanol production through process optimization is a simpler, easier, and novel method for commercialization.

Keywords Magnetic nanoparticles, Optimization, Hydrolysis, Agar, Bioethanol

Introduction

Agar is the key component of the cell walls of certain red algae, such as *Gelidium* and *Garcilaria* [1, 2], which is composed of the polysaccharides agarose and porphyrin [3]. Porphyran consists of a porphyrobiose repeating unit (G-L6S) of -L-galactose-6-sulfate, whereas agarose is a linear polysaccharide composed of an agarobiose repeating unit (G-AHG) of -D-galactose and -L-galactose-3,6-anhydro [4, 5]. Agar is subsequently used as a gelling agent [6] that possesses a variety of biological properties, such as in microbial cultivation and vegetable tissue culture, and may be employed in a wide range of commercial applications, including the food, cosmetics, and pharmaceutical sectors [7]. In addition, agar monomeric sugars, such as D-galactose, 3,6-anhydro-L-galactose,

*Correspondence:
Jung-Ho Park
jungho@kribb.re.kr
[1] Bio-Evaluation Center, Korea Research Institute of Bioscience and Biotechnology, Cheongju 28116, Republic of Korea
[2] 4D Convergence Technology Institute (National Key Technology Institute in University), Korea National University of Transportation, Jungpyeong 27909, Republic of Korea
[3] Department of Food Science and Technology, Chungnam National University, Daejeon 34134, Republic of Korea
[4] Department of Biosystems and Bioengineering, KRIBB School of Biotechnology, Korea University of Science and Technology (UST), 217 Gajeong-Ro, Yuseong-Gu, Daejeon, Korea

and L-galactose-6-sulfate, can be functionalized for a variety of biorefineries or biofuel generation [8].

To address a variety of challenges, including the depletion of fossil fuel reserves and greenhouse gas (GHG) emissions, biofuels, such as bioethanol obtained from the synthesis of algal biomass, may be considered a practical substitute for fossil fuels [9–11]. Compared with lignocellulosic biomass, algal biomass (agar) comprises a high concentration of polysaccharides and lipids free of lignin, easing hydrolysis [12, 13]. Although biofuel production using the agar substrate is the most eco-friendly process, the difficulties associated with it must be avoided for industrial use. The hysteresis properties of agar complicate its use, which has been addressed using different approaches, including physiochemical pretreatment processes, such as microwave-assisted hydrothermal technology [14], deep eutectic solvent (DES) [15], alkaline pretreatment [16], acid catalyst pretreatment [17], synthetic biology [18], and genetic engineering [5]. Because it solidifies with adding water, chemical liquefication and enzymatic saccharification can be alternatives for generating fermentable monosugars. Different physiochemical techniques have been employed to degrade the algal polymer structure to liberate the fermentable monosugars for subsequent enzymatic hydrolysis [19–22] by releasing inhibitory compounds, such as hydroxymethyl furfural (HMF), a phenolic molecule that can prevent microbial fermentation [23, 24]. Meanwhile, the use of biological pretreatments, such as microbial strains and enzymes for agar degradation, is preferable, because it requires less energy, produces no inhibitors, and requires ambient working conditions [25]. However, biological approaches have several limitations, such as a high cost, limited necessity for biocatalysts, and stability. These difficulties with the physicochemical and biological agar degradation methods limit their use in the development of eco-friendly and successful pretreatment methods for agar feedstocks [26].

Owing to their distinctive characteristics, such as large surface area, high surface to volume ratio, ease of isolation, and electro conductivity, nanoparticles (NPs) have recently been used as substitutes for enzyme-mimicking behavior (also known as nanozymes) in a variety of fields, including agriculture, biofuels, and biomedicine [27]. It is possible to alter the size, shape, and doping of enzyme-mimicking NPs to modify their properties. Several nanomaterials (Co_3O_4, Fe_3O_4, Pt, Ag, Au, Zn, CeO_2) have been identified for enzyme-mimicking activities, including those of peroxidase, oxidase, and catalase [28]. Fe-based NPs have demonstrated distinctive enzyme-mimicking properties and magnetic behaviors [29]. Pena et al. executed two separate magnetic nanoparticles (MNPs) incorporating different acid functions to demonstrate the considerable catalytic hydrolysis of wheat straw [30].

Considering the aforementioned, the synthesized Fe_3O_4-MNPs were employed for the pretreatment of agar substrates in the presence of hydrogen peroxidase (H_2O_2) and bioethanol fermentation in this study. *Escherichia coli* and *Saccharomyces cerevisiae* strains were used for bioethanol production through the consolidated bioprocessing of pretreated agar, which significantly reduced the overall cost of the agar substrate for bioethanol production. Many studies related to bioethanol production have been conducted using carbohydrate sources present in algal biomass [31]. Various structural characterization methods, such as Fourier transform infrared (FTIR), field emission scanning electron microscopy (FESEM), transmission electron microscopy (TEM), energy dispersive spectroscopy (EDS), X-ray power diffraction (XRD), and thermogravimetric analysis (TGA) of the untreated and Fe_3O_4-MNP-treated agar were utilized to validate the efficiency of the Fe_3O_4-MNPs-mediated degradation of agar in a sustainable manner. Furthermore, a central composite design (CCD) for the optimization process was applied to determine various operating parameters. An analysis of variance was used to determine the individual and interaction effects of these parameters. Thus far, several studies have been reported regarding bioethanol fermentation using nanomaterials in several steps. However, in this study, Fe_3O_4-MNPs were used for pretreatment, followed by fermentation without enzymatic saccharification, thereby reducing the use of enzymes. To the best of our knowledge, the application of agar pretreatment using Fe_3O_4-MNPs without enzymes through process optimization (CCD) for bioethanol production has not been reported relative to the current development of biorefineries. The use of nanoparticles for the hydrolysis of agar for bioethanol production is considerably feasible and can decrease the environmental impact, as NPs can be extracted from marine sources, such as seaweed.

Results and discussion

Estimation of the nanoparticle concentration, hydrogen peroxide concentration, and effect of temperature on reducing the sugar production

First, the concentration of nanoparticles in high-reducing sugar products was evaluated using various MNP concentrations (0.1%, 0.5%, and 1%). At each of these three concentrations, 1% of MNPs produced 0.052 g/L of reducing sugar from 10 g/L (1%) agar when only dH_2O was used (Fig. 1). In addition, citrate buffer (CB pH 6.2) at two different concentrations (0.1 and 0.5 M) was employed to improve the synthesis of reducing sugars (Fig. 2). Notably, approximately 0.1 g/L (1.9-fold) of

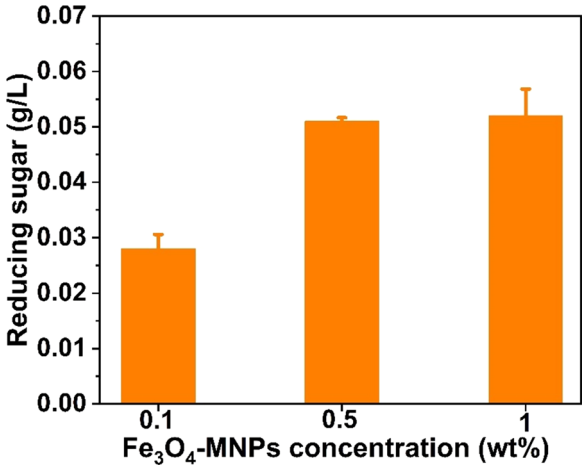

Fig. 1 Comparison on the reducing sugar production when different concentration (0.1%, 0.5%, and 1%) of Fe_3O_4-MNPs was used in presence of distilled water (DW) as catalytic solvent

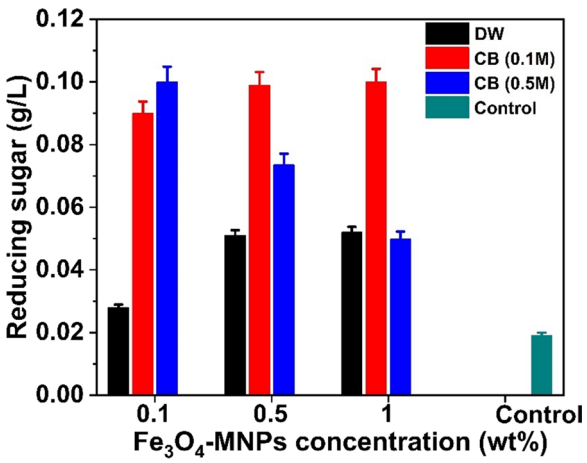

Fig. 2 Comparison on the reducing sugar production with (0.1%, 0.5%, and 1%) Fe_3O_4-MNPs and without (Control) Fe_3O_4-MNPs in presence of distilled water (DW) and citrate buffer (CB, pH6.2), respectively

reducing sugar was achieved when 0.1 M of citrate buffer (pH 6.2) along with 0.1% of MNPs were used, whereas it decreased when 0.5% and 1% of MNPs were used, as illustrated in Fig. 2. Nanoparticles at higher concentrations are difficult to distribute in water owing to their ferromagnetic characteristics (Fe_3O_4-MNPs) and require many washing processes for further saccharification of the pretreated biomass [32]. Therefore, a higher concentration of nanoparticles (Fe_3O_4-MNPs) for pretreatment is not feasible on an industrial scale. Considering different concentrations of hydrogen peroxide (100, 250, and 500 mg/L) along with 0.1 M CB (pH6.2) (Fig. 3a), nearly 0.903 g/L (21-fold) of reducing sugar was obtained when 500 mg/L hydrogen peroxide was used (Fig. 3b). Hydrogen peroxidase can generate free radicals in the presence of hydrogen peroxidase, which help in the degradation of agar to release fermentable sugar. Finally, the effects of temperature (30, 40, 50, and 60°C) on reducing the sugar production were examined using the aforementioned combinations. Among these, a high-reducing sugar was produced at 30 °C, as shown in Fig. 4. Based on these results, we designed the experiments using the response surface methodology (RSM) for bioethanol production.

Optimization of bioethanol production and its interaction using RSM

Bioethanol production was optimized using RSM, where a central composite design (CCD) full factorial design matrix, each with 20 individual runs for *Escherichia coli* K12 and *Saccharomyces cerevisiae* S288c ATCC 7754, is provided in Table 1a, b, respectively. Based on the response values, the bioethanol production ranged from 0.0018% (run no. 4) to 0.0042% (run no. 3) for *Escherichia coli* K12, and 0.002% (run no. 17) to 0.181% (run no. 1) for *Saccharomyces cerevisiae* S288c ATCC 7754. The response variables that corresponded to the coded values of the variables were adjusted to the quadratic model, as provided in Eq. (4). The linear, square, and interaction coefficients with coded p and t values are shown in Tables 2a for *Escherichia coli* K12 and (b) for *Saccharomyces cerevisiae* S288c ATCC 7754. The derived quadratic polynomial equation in terms of the coded variables, which characterizes the interaction between the independent variables and the response factor, is as follows:

$$\text{For } \textit{Escherichia coli}\text{: } Y_{\textit{bioethanol production}}\ (\%) = 0.0263 + 0.0000015X_1^2 - 0.000019X_2^2 + 0.000012X_3^2 \quad (1)$$

$$\text{For } \textit{Saccharomyces cerevisiae}\text{: } Y_{\textit{bioethanol production}}\ (\%) = 0.059 - 0.00112X_1 - 0.0023X_2 + 0.0034X_3 + 0.000018X_1X_2 \quad (2)$$

where Y denotes the bioethanol production (%), and $X1$, $X2$, and $X3$ are the coded values of the independent variables, as shown in Table 6.

Analysis of variance (ANOVA)

Model significance in quadratic terms was estimated using the t test, F value, and p value. A higher t test value indicates a greater significant coefficient of the model, whereas a p value < 0.05 represents the excellent significance of the response variables. Table 3 presents the ANOVA results of the quadratic models. In addition, the F values (4.71 for *Escherichia coli* K12 and 14.64 for

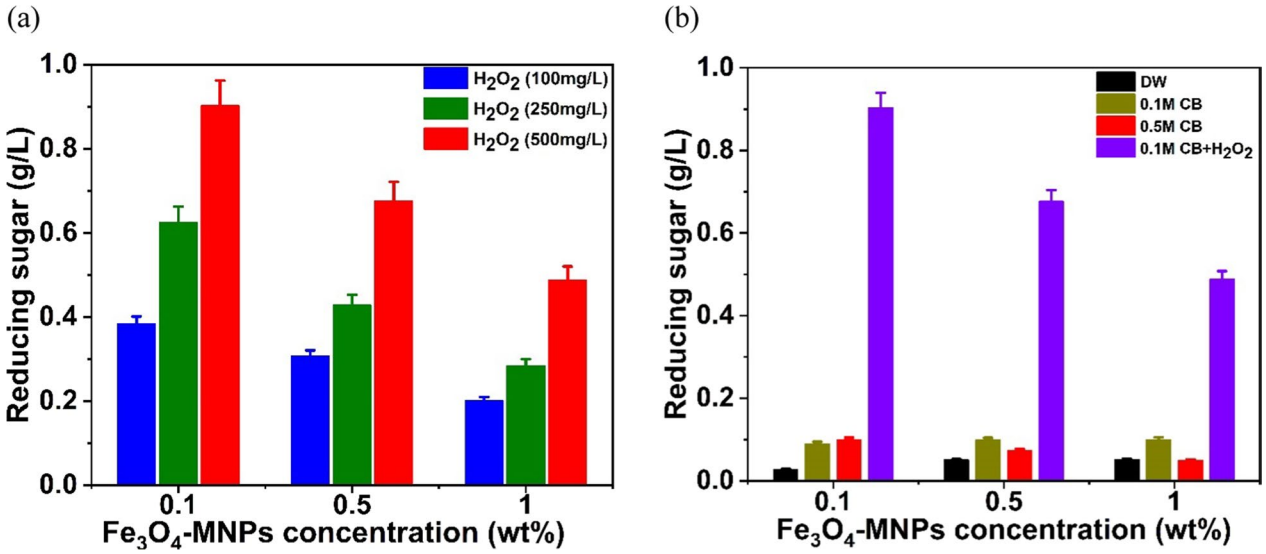

Fig. 3 Estimation of reducing sugar production when different concentration (100, 250, and 500 mg/L) of hydrogen peroxide was used (**a**) and with the combination of citrate buffer (CB) and 500 mg/L hydrogen peroxide (**b**)

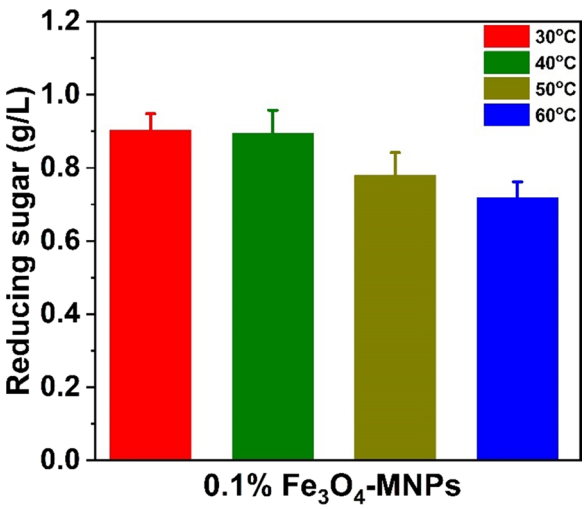

Fig. 4 Illustration on reducing sugar production at different (30, 40, 50, and 60 °C) temperatures

Saccharomyces cerevisiae S288c ATCC 7754) and *p* values (0.00001) indicated that the model was highly significant. The correlation coefficient (R^2) value of 0.90 for *Escherichia coli* K12 and 0.92 for *Saccharomyces cerevisiae* S288c ATCC 7754 indicated a similarity between the experimental and predicted values of the response; greater R^2 values affirm the model.

Process variables through interaction effects

A 3D surface plot illustrates the synergistic effect of the two process variables on the efficiency of bioethanol production (Fig. 5). An increase in the hydrolysate concentration and temperature resulted in an increase in the bioethanol production efficiency for *Saccharomyces cerevisiae* S288c ATCC 7754 (Fig. 5a), whereas considering time and temperature (Fig. 5b), increases in both response variables exhibited a positive influence on the bioethanol production efficiency. Similarly, an increase in the reaction time and hydrolysate concentration also elucidated an increase in the bioethanol production efficiency, as shown in Fig. 5c. Overall, an increase in the process variables positively influenced bioethanol production.

For *Escherichia coli* K12, an increase in the hydrolysate concentration and temperature resulted in an increase in the bioethanol production efficiency up to a certain point, followed by a decrease in the bioethanol production with a further increase in the hydrolysate concentration (Fig. 5d). Similarly, the interaction between the time and temperature is illustrated in Fig. 5e. An increase in the reaction time resulted in a decrease in the bioethanol concentration, whereas an increase in temperature resulted in an increase in the bioethanol concentration. Furthermore, the effects of the reaction time and hydrolysate concentration are illustrated in Fig. 5f. The bioethanol production efficiency increased as the hydrolysate concentration and reaction time increased. This indicates that an increase in temperature enhanced the overall bioethanol concentration. In addition, a higher hydrolysate concentration may lead to exhaustion of the carbon source, leading to continuous bacterial growth.

Table 1 Central composite design matrix of optimization variables with actual values and response variable for ethanol production

Run	Hydrolysate concentration (%)	Temperature °C	Time H	Ethanol concentration (%)	
				Actual value	Predicted value
(a) *Escherichia coli* K12					
1	1.47759	33.5	5.5	0.0023	0.0026
2	22.5	33.5	5.5	0.0020	0.0020
3	35	30	8	0.0042	0.0040
4	10	37	3	0.0018	0.0016
5	22.5	33.5	5.5	0.0020	0.0020
6	22.5	33.5	5.5	0.0020	0.0020
7	22.5	33.5	1.29552	0.0020	0.0023
8	22.5	33.5	9.70448	0.0019	0.0022
9	10	37	8	0.0021	0.0019
10	22.5	27.6137	5.5	0.0023	0.0025
11	43.5224	33.5	5.5	0.0025	0.0028
12	10	30	3	0.0035	0.0033
13	35	37	8	0.0023	0.0021
14	35	30	3	0.0024	0.0022
15	22.5	39.3863	5.5	0.0025	0.0028
16	10	30	8	0.0027	0.0025
17	22.5	33.5	5.5	0.0020	0.0020
18	22.5	33.5	5.5	0.0020	0.0020
19	22.5	33.5	5.5	0.0020	0.0020
20	35	37	3	0.0027	0.0025
(b) *Saccharomyces cerevisiae* S288c (ATCC 7754)					
1	10	30	8	0.0181	0.0163
2	22.5	35	5.5	0.0056	0.0056
3	35	40	8	0.0022	0.0027
4	22.5	35	9.7	0.0071	0.0071
5	22.5	35	1.29	0.0046	0.0043
6	22.5	35	5.5	0.0056	0.0056
7	22.5	43.409	5.5	0.0054	0.0033
8	10	40	3	0.0064	0.0065
9	35	30	8	0.0072	0.0073
10	43.5224	35	5.5	0.0051	0.0043
11	10	30	3	0.0119	0.0116
12	22.5	35	5.5	0.0056	0.0056
13	22.5	26.591	5.5	0.0097	0.0115
14	22.5	35	5.5	0.0056	0.0056
15	22.5	35	5.5	0.0056	0.0056
16	1.47759	35	5.5	0.0135	0.014
17	35	40	3	0.002	0.004
18	10	40	8	0.0059	0.0072
19	22.5	35	5.5	0.0056	0.0056
20	35	30	3	0.0058	0.0047

Optimization of the process variables for bioethanol production using *Saccharomyces cerevisiae* S288c (ATCC 7754) and *Escherichia coli* K12 was conducted (as depicted in Table 1a, b), which demonstrated that when *Saccharomyces cerevisiae* S288c (ATCC 7754) was used, bioethanol production was comparatively higher than *Escherichia coli K12*. This is because *Saccharomyces cerevisiae* S288c (ATCC 7754) is known to utilize galactose

Table 2 Results of central composite design for ethanol concentration

Model term	Coefficient estimate	Computed *t* value	*p* Value
(a) Model coefficients, *t* and *p* value for second-order regression model for *Escherichia coli* K12			
Intercept (β_0)	0.001986	8.73	0.000*
Linear coefficients			
X_1 (Hydrolysate concentration %)	0.000226	0.89	0.394
X_2 (Temperature °C)	− 0.000439	− 1.73	0.115
X_3 (Time H)	0.000090	0.35	0.730
Square coefficients			
X_1^2 (Hydrolysate concentration % x Hydrolysate concentration %)	0.000667	1.60	0.140
X_2^2 (Temperature °C x Temperature °C)	0.000667	1.60	0.140
X_3^2 (Time H x Time H)	0.000217	0.52	0.613
Interaction coefficients			
X_1X_2 (Hydrolysate concentration % x Temperature °C)	0.000247	0.44	0.667
X_1X_3 (Hydrolysate concentration % x Time H)	0.000672	1.20	0.256
X_2X_3 (Temperature °C x Time H)	− 0.000389	− 0.70	0.502
(b) Model coefficients, *t* and *p* value for second-order regression model for *Saccharomyces cerevisiae* S288c (ATCC 7754)			
Intercept (β_0)	0.005606	9.93	0.000 *
Linear coefficients			
X_1 (Hydrolysate concentration %)	− 0.004829	− 7.67	0.000 *
X_2 (Temperature °C)	− 0.004151	− 6.59	0.000 *
X_3 (Time H)	0.001417	2.25	0.048 *
Square coefficients			
X_1^2 (Hydrolysate concentration % x Hydrolysate concentration %)	0.00355	3.45	0.006 *
X_2^2 (Temperature °C x Temperature °C)	0.00180	1.75	0.111
X_3^2 (Time H x Time H)	0.00010	0.10	0.922
Interaction coefficients			
X_1X_2 (Hydrolysate concentration % x Temperature °C)	0.00315	2.27	0.046 *
X_1X_3 (Hydrolysate concentration % x Time H)	− 0.00145	− 1.05	0.319
X_2X_3 (Temperature °C x Time H)	− 0.00279	− 2.02	0.071

and glucose, which is formed sequentially from agar hydrolysis, and can also tolerate a wide range of pH values [33, 34], whereas *Escherichia coli* K12 can only utilize glucose. Ethanol production using the synthesized Fe_3O_4-MNPs was comparatively lower (Table 4) than the simultaneous enzymatic hydrolysis. Not using bacterial enzymes for the hydrolysis of agar results in a low ethanol yield, despite the simultaneous saccharification of biomass with enzymes enhancing the reducing sugar production, as reported in other studies [35–37]. However, considering the cost limitations, which are assumed to account for approximately 20% of the ethanol production costs [36], slow reaction rate resulting in a time-consuming hydrolysis, and difficulty in enzyme recovery, the enzymatic hydrolysis process remains under consideration [38, 39]. Byproducts formed during hydrolysis, such as furfural, HMF, and formic acid, inhibit enzymatic activity [40, 41]. In addition, enzymatic degradation may occur after thermal hydrolysis, leading to researchers focusing on developing thermostable enzymes [42]. Therefore, the use of the synthesized Fe_3O_4-MNPs for bioethanol production can be a new and feasible method. Using synthesized Fe_3O_4-MNPs in the absence of bacterial cells has a limited hydrolysis potential for agar, which ultimately reduces the release of monosugars. However, considering certain other prospective studies, using only Fe_3O_4-MNPs can be a new strategy to overcome the drawbacks possessed by other (chemical, hydrothermal, and enzymatic) hydrolysis techniques.

Experimental validation

The consistency of the model between the individual experiments and process optimization conditions were tested according to those predicted by the CCD analysis in response to the bioethanol concentration. Table 5 exhibits the optimum process conditions and bioethanol production, where the final bioethanol production obtained after the experiment run with the predicted variables was recorded as 0.003 for *Escherichia coli* K12 and 0.072 for *Saccharomyces cerevisiae* S288c ATCC

Table 3 Estimation of analysis of variance for regression expression

Source	DF	SS	MS	*f* value	*p* value
(a) ANOVA for quadratic model *Escherichia coli* K12					
Regression	13	0.000003	0.000000	4.17	0.0447*
X_1 (Hydrolysate concentration %)	1	0.000000	0.000000	0.1863	0.6811
X_2 (Temperature °C)	1	0.000001	0.000001	0.2054	0.6663
X_3 (Time H)	1	0.000000	0.000000	0.0466	0.8363
X_1^2	1	0.000001	0.000001	2.57	0.0339*
X_2^2	1	0.000001	0.000001	2.57	0.0348*
X_3^2	1	0.000000	0.000000	0.27	0.04061*
X_1X_2	1	0.000000	0.000000	0.20	0.667
X_1X_3	1	0.000000	0.000000	1.45	0.256
X_2X_3	1	0.000000	0.000000	0.49	0.502
Residual (Error)	10	0.000003	0.000000		
Lack-of-Fit	1	0.000003	0.000001	*	*
Pure Error	5	0.000000	0.000000		
Total	19	0.000006			
(b) ANOVA for quadratic model *Saccharomyces cerevisiae* S288c (ATCC 7754)					
Regression	9	0.00003	0.000000	14.64	0.0001*
X_1 (Hydrolysate concentration %)	1	0.00001	0.00001	58.82	< 0.0001*
X_2 (Temperature °C)	1	0.00001	0.00001	43.45	< 0.0001*
X_3 (Time H)	1	0.00001	0.00001	5.06	0.048*
X_1^2	1	0.000000	0.000000	11.87	0.006*
X_2^2	1	0.000006	0.000006	3.05	0.111
X_3^2	1	0.000000	0.000000	0.01	0.8854
X_1X_2	1	0.00001	0.00001	5.17	0.046*
X_1X_3	1	0.000002	0.000002	1.10	0.319
X_2X_3	1	0.000008	0.000008	4.08	0.071
Residual (Error)	10	0.000019	0.000002		
Lack-of-Fit	5	0.000019	0.000004	*	*
Pure Error	5	0.000000	0.000000		
Total	19	0.0002	0.000000	14.40	0.0001*

DF: degree of freedom, SS: sum of square, and MS: mean square

*Significant $p \leq 0.05$

7754. The precise variable concentration for the bioethanol production efficiency was determined using process-variable optimization.

Characterization of Fe_3O_4-MNPs and agar

An SEM analysis was used to morphologically characterize Fe_3O_4-MNPs and agar before and after processing; the resulting images are displayed in Fig. 6a–c, respectively. As shown in Fig. 6a, the surface morphology of Fe_3O_4-MNPs demonstrates a spherical form [43]. Similarly, the agar surface morphology before pretreatment demonstrated a solid rigid structure (Fig. 6b); however, the surface morphology after pretreatment exhibited a disruption of the surface (Fig. 6c), because the magnetic iron nanoparticles (Fe_3O_4-MNPs) have the ability to produce reactive oxygen species (ROS) via the Fenton reaction from H_2O_2, causing oxidative stress and ultimately damaging the cell wall of the agar. In addition, TEM image of Fe_3O_4-MNPs exhibits a spherical shape with a uniform diameter in range of 8–10 nm (Fig. 6d) corelated with the reported one [44].

Energy dispersive spectroscopy (EDS) and field-emission SEM were employed to determine the elemental composition of the synthesized Fe_3O_4-MNPs and agar before and after pretreatment (Fig. 7). Figure 7a–c presents the typical EDS spectra of the synthesized Fe_3O_4-MNPs with 62.38% Fe and 27.36% O, indicating that the primary components of the nanoparticles are iron and oxygen [32]. Similarly, Fig. 7d–f illustrates the EDS analysis of agar before pretreatment, demonstrating

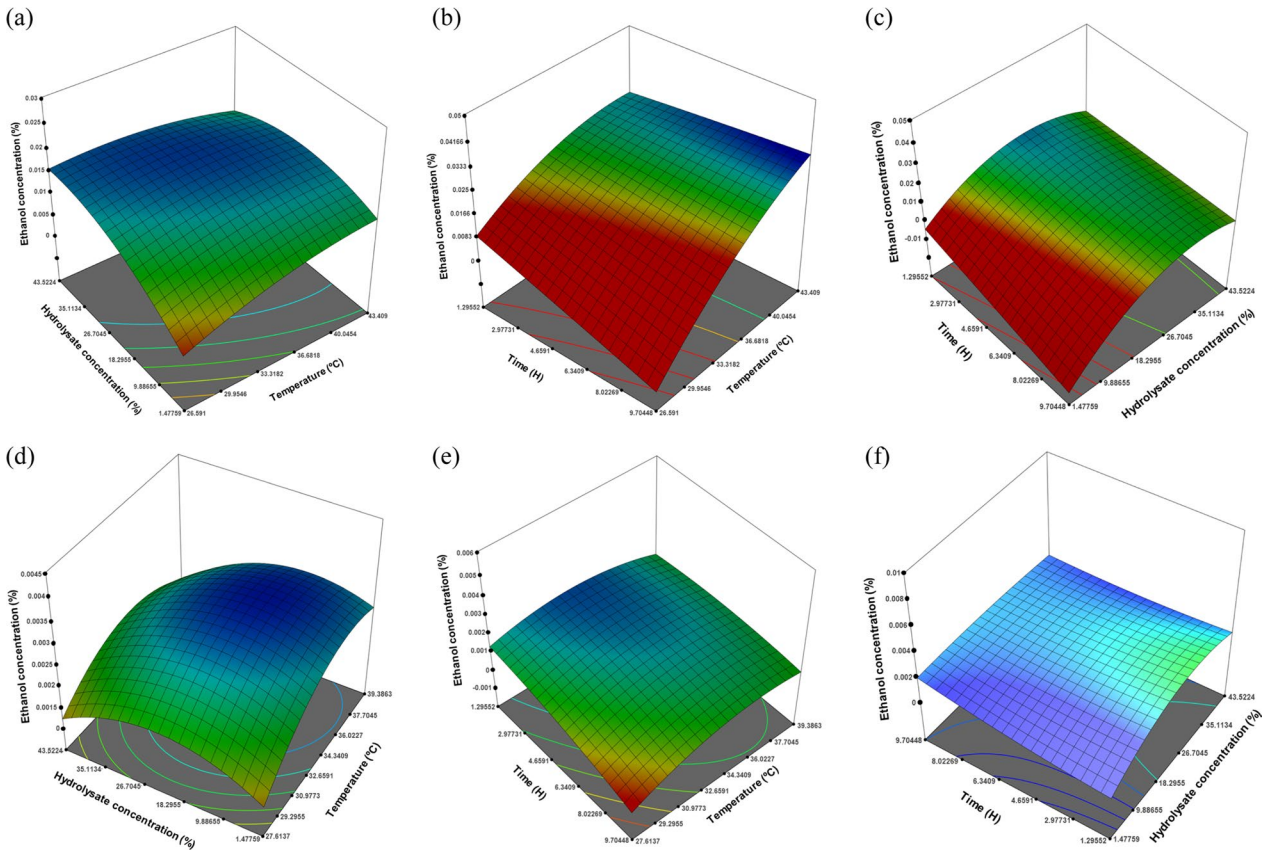

Fig. 5. 3D plots depicting interactions among different process variables; (**a**, **d**) hydrolysate concentration (%), temperature (°C); (**b**, **e**) time (H), temperature (°C) and (**c**, **f**) time (H), hydrolysate concentration (%) for both *Saccharomyces cerevisiae* and *Escherichia coli*

a maximum of 49.75% C and 48.36% O, and 50.96% C and 48.24% O. Likewise, Fig. 7g–i demonstrates the EDS analysis of agar after pretreatment, where the vanishing of Cl (Fig. 7i) indicates the C–O of carbohydrate in agar.

The characteristic functional groups of the synthesized Fe_3O_4-MNPs and agar before and after pretreatment were determined by the FTIR analysis (Fig. 8a), which demonstrates a sharp peak at 593 cm^{-1} related to the stretching vibration of Fe–O from magnetite, which also denotes the purity of the nanoparticles [45]. Similarly, the broad peak at 3436 cm^{-1} corresponds to the –OH stretching vibration of the hydrogen bond of absorbed water on the surface of the nanoparticles [46]. The peak at 2922 cm^{-1} indicates the asymmetric stretching of C–H and the peak at 1625 cm^{-1} indicates the bending (δ) vibrations of the H—O—H groups [46, 47].

In Fig. 8b, the broad peak at 3324 cm^{-1} before and after pretreatment demonstrates the stretching vibration of –OH, indicating the presence of the hydroxyl group in agar [48], whereas after pretreatment, the peak shrinks, indicating the hydrolysis of agar. Furthermore, the peak at 2927 cm^{-1} before and after pretreatment corresponds to the C–H stretching vibrations of the $-CH_3$ and $-CH_2$ groups [49, 50]. The adsorption band at 1654 cm^{-1} attributed to the C=O and N–H stretching groups indicates the formation of conjugated peptides bonds [51]. In addition, the peak at 1362 cm^{-1} corresponds to the asymmetric bending stretching of –C–H to $-CH_3$ [52], whereas the peaks at 1142 cm^{-1} and 1074 cm^{-1} correspond to the C–O–C stretching vibration of polysaccharides and the C–O stretching vibration of carbohydrates, respectively [53]. In addition, the peak at 933 cm^{-1} indicates the presence of a 3,6-anhydrous galactose bridge, confirming the agar composition [54, 55].

Figure 9 presents the XRD patterns of the synthesized Fe_3O_4-MNPs and agar before and after pretreatment. Regarding the diffraction planes of the Fe_3O_4-MNPs spinel structure, a succession of distinctive peaks was observed in the XRD pattern at 2θ of 30.04°, 35.4°, 43.02°, 57.06°, and 62.54°, corresponding to the diffraction planes of (220), (311), (400), (511), and (440), respectively, demonstrating the reflections of magnetite (Fig. 9a) and indicating the presence of the crystalline spinel-structured magnetite (Fe_3O_4-MNPs) phase

Table 4 Comparison of ethanol yield using different hydrolysis technique in presence of different substrates

Feedstock	Config	Microorganisms	EtOH	References
U. fasciata (green)	EH, SHF	*Saccharomyces cerevisiae* MTCC 180	47 (g/100 g)	[68]
U. fasciata (green)	EH, SHF	*Saccharomyces cerevisiae*	47 (g/100 g)	[69]
Gracilaria sp. (red)	AH & EH, SHF	*Saccharomyces cerevisiae* Wu	47 (g/100 g)	[70]
G. amansii (red)	AH, SHF	*Brettanomyces custersii*	38 (g/100 g)	[71]
L. japonica (brown)	AH & EH, SHF	*Escherichia coli* KO11	41 (g/100 g)	[72]
K. alvarezii (red)	AH, SSF	Brewer's yeast	21 (g/100 g)	[73]
Sargassum sagamianum (brown)	TH & EH, SHF	*P. stipites* CBS7126	44 (g/100 g)	[74]
E. globulus	SSF	*Saccharomyces cerevisiae* IR2T9	30–38 (g/L)	[75]
NS	CBP	*Saccharomyces cerevisiae* MT8-1	0.71 (g/L)	[76]
Raw CC	SPS using Ce–Fe_3O_4, EH	*Saccharomyces cerevisiae*	21.7 g/L	[77]
Recycled paper sludge	Batch/SHF	*Saccharomyces cerevisiae* PE-2	5.6–6.3 g/L	[78]
E. globulus	SSF	*Saccharomyces cerevisiae* D5A	5.67 g/L	[79]
Sugarcane bagasse	Phosphoric acid pretreatment	*Escherichia coli* MM170	0.25–0.27 (g/g raw biomass)	[80]
Lodgepole pine	SPORL pretreatment	NS	0.22 (g/g raw biomass)	[81]
Birch	Alkaline	NS	0.11 (g/g raw biomass)	[82]
Miscanthus	LHW	NS	0.15 (g/g raw biomass)	[83]
Agar	SPS using Fe_3O_4-MNPs	*Saccharomyces cerevisiae* S288c (ATCC 7754)	0.0181%	This study
Agar	SPS using Fe_3O_4-MNPs	*Escherichia coli* K12	0.0042%	This study

EtOH: ethanol production, EH: enzymatic hydrolysis, AH: acid hydrolysis, TH: thermal hydrolysis, SHF: separate hydrolysis and fermentation, SSF: simultaneous saccharification and fermentation, CBP: consolidated bioprocessing, SPS: simultaneous pretreatment and saccharification, LHW: liquid hot water, SPORL: sulfite pretreatment to overcome recalcitrance of lignocellulose, CC: Corn cob, NS: not specified

Table 5 Global optimum values of variables with predicted and actual response

Hydrolysate concentration (%)	Temperature (°C)	Time (H)	Ethanol concentration (%)	
			Predicted	Actual
(a) *Escherichia coli* K12				
35	27.6	9.7	0.0225	0.003
(b) *Saccharomyces cerevisiae* S288c (ATCC 7754)				
1.47	26.6	9.7	0.225	0.072

of iron oxide, similar to that reported previously [56]. Similarly, the XRD pattern of agar before pretreatment indicating a peak at $2\theta = 18.18^{o}$, 39.28^{o}, and 61.32^{o} (Fig. 9b) defined the hydrated crystalline structure and accordingly, the presence of an amorphous structure [48]. In contrast, the broad peak shifted at $2\theta = 15.59^{o}$ (Fig. 9c), indicating the increased release of the amorphous structures owing to the corrosion of the synthesized Fe_3O_4-MNPs, further promoting the release of reducing sugar.

A TGA analysis of the pyrolytic properties of the synthesized Fe_3O_4-MNPs and agar before and after pretreatment is shown in Fig. 10. The TGA curve of Fe_3O_4-MNPs shown in Fig. 10a demonstrates four phases of weight loss, where the first weight loss was observed between 30 and 130 °C with a mass loss of 1.7%. This was owing to the loss of the absorbed physical and chemical water from the surface of the NPs [57]. Furthermore, a second weight loss of 0.4% was observed between 130 and 200 °C, which corelated with the existence of certain combustible products in the sample. This loss of water from the sample was verified by the dips at 75 and 235 °C in the DTG curve. Similarly, a third weight loss of 1.2% was observed between 200 and 270 °C, resembling the complete rapid decomposition of the water residual as the first two steps. Finally, a 2.4% weight loss was observed at 270–560 °C, and as a dip at 515 °C in the DTG curve.

Regarding agar before the pretreatment, the first weight loss of 11% was observed between 30 and 100 °C, which was owing to the evaporation of free and bound water (Fig. 10b) [48]. Similarly, the weight loss of 7% in the second stage was observed owing to the remaining moisture in the sample. During the third stage, a maximum decomposition occurred with a weight loss of 55% between 270 and 450 °C. At this stage, higher molecular compounds such as carbohydrates, proteins, and lipids in the agar underwent cracking and depolymerization reactions owing to the continuous supply of heat [48]. This was verified by the dips at 260 and 745 °C in the

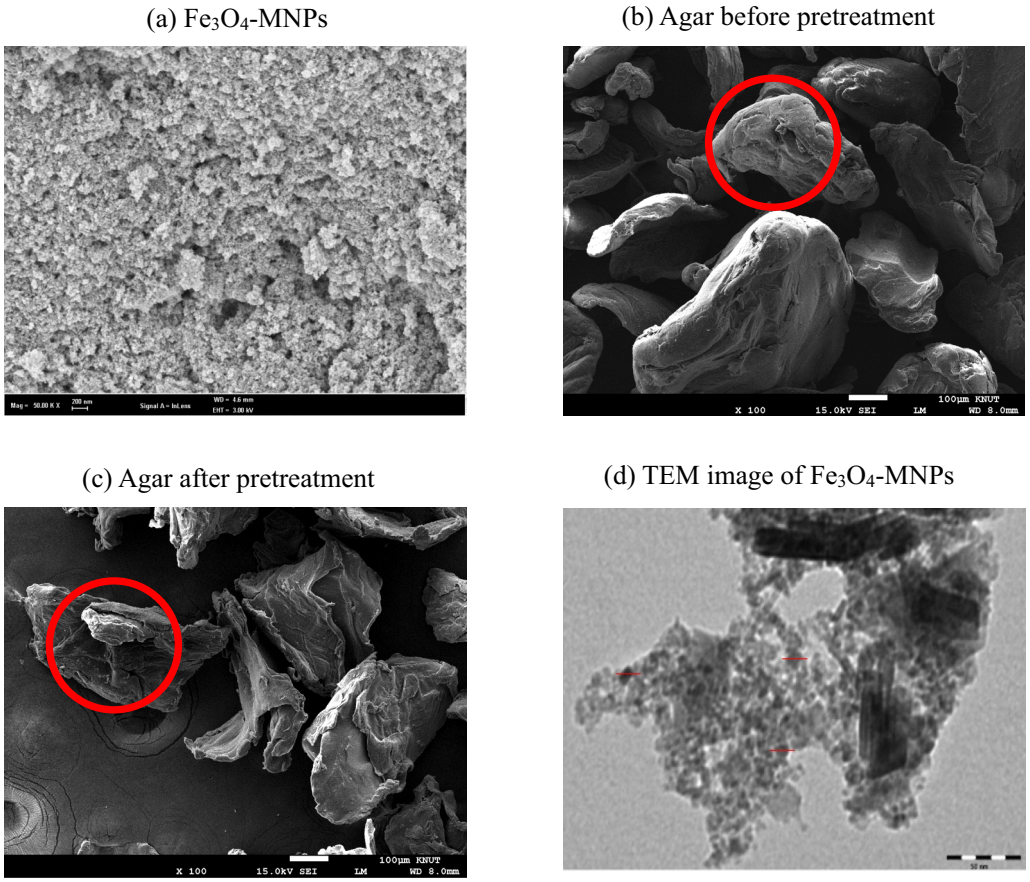

Fig. 6 Morphology characterization of synthesized Fe3O4-MNPs. **a** SEM analysis of synthesized Fe_3O_4-MPNs, **b** SEM image of agar before pretreatment, **c** SEM image of agar after pretreatment with 0.1% Fe_3O_4-MNPs, 500 mg/L H_2O_2 and citrate buffer (CB) (pH6.2), and (**d**) TEM image of synthesized Fe_3O_4-MNPs

DTG curve. Moreover, the third stage is considered an active pyrolytic zone, because it refers to the production of biofuels and is comparatively similar to that previously reported [58, 59].

Furthermore, Fig. 10c exhibits the pyrolytic properties of agar after pretreatment, where 14% of weight loss was observed between 30 and 100 °C followed by a 4% weight loss between 100 and 260 °C. Approximately 56% of weight loss was observed, which was slightly more than that before pretreatment (Fig. 10b) owing to the decomposition of higher compounds, such as polysaccharides, proteins, and lipids, due to the catalytic behavior of the synthesized Fe_3O_4-MNPs. At temperatures greater than 700 °C, no significant weight loss was observed, mostly owing to the presence of the inorganic content in the agar [60].

Materials and methods

Materials

Ferric chloride ($FeCl_3$) and ferrous chloride ($FeCl_2$) were purchased from Junsei Chemicals Co. Ltd., Japan. Hydrogen peroxide (H_2O_2, 34.5%) and the ammonia solution (20–35%) were purchased from Samchun Chemicals Co. Ltd., Korea. Sodium Citrate dihydrate ($C_6H_9Na_3O_9.2H_2O$) and Citric Acid ($C_6H_8O_7$) (Sigma-Aldrich) were purchased, as well as Agar (Bacto™), LB broth, and the YM broth (Difco™).

Synthesis of iron oxide MNPs (Fe_3O_4-MNPs)

Fe_3O_4-MPNs were chemically synthesized, as described by Maharjan et al. [57], by combining 3 mol of ferric chloride ($FeCl_3$) and 1 mol of ferrous chloride ($FeCl_2$) in deionized water. Subsequently, an equal volume of ammonia solution was added dropwise and stirred at 60 °C overnight (Fig. 11). The synthesized Fe_3O_4-MNPs were centrifuged at 15,000 rpm at 4 °C for 30 min, followed by washing with deionized water at least three times and then freeze-dried until an equal dry weight was obtained.

(a) Fe_3O_4-MNPs

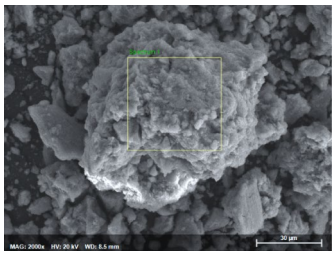

(b)

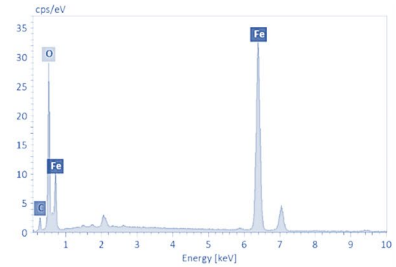

(c)

Spectrum 1

Element	At. No.	Mass [%]	Mass Norm. [%]	Atom [%]	abs. error [%] (3 sigma)
C	6	5.97	6.23	14.94	2.80
O	8	27.36	28.59	51.45	9.42
Fe	26	62.38	65.18	33.60	5.04
		95.71	**100.00**	**100.00**	

(d) Agar before pretreatment

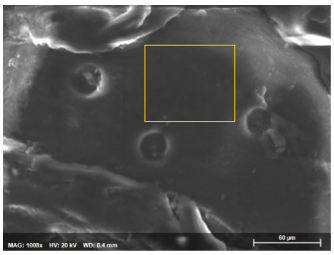

(e)

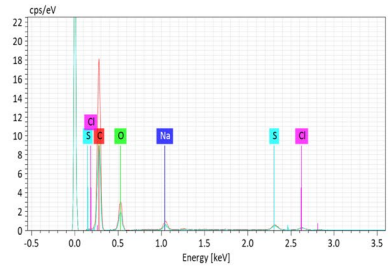

(f)

SPU0

Element	At. No.	Mass [%]	Mass Norm. [%]	Atom [%]	abs. error [%] (3 sigma)
C	6	49.75	49.75	57.24	16.78
O	8	48.36	48.36	41.77	16.65
Na	11	1.07	1.07	0.64	0.29
S	16	0.55	0.55	0.24	0.14
Cl	17	0.27	0.27	0.10	0.11
		100.00	**100.00**	**100.00**	

(g) Agar after pretreatment

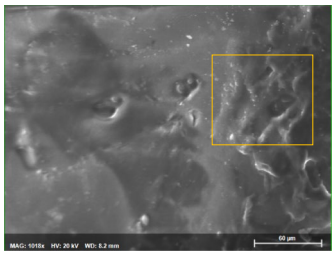

(h)

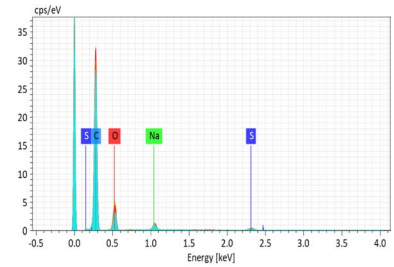

(i)

SPU0

Element	At. No.	Mass [%]	Mass Norm. [%]	Atom [%]	abs. error [%] (3 sigma)
C	6	50.96	50.96	58.21	16.72
O	8	48.24	48.24	41.36	16.18
Na	11	0.51	0.51	0.31	0.18
S	16	0.28	0.28	0.12	0.11
		100.00	**100.00**	**100.00**	

Fig. 7 FESEM and EDS analysis of; (**a**–**c**) synthesized Fe_3O_4-MNPs, (**d**–**f**) agar before pretreatment, and (**g**–**i**) agar after pretreatment

(a) Fe_3O_4-MNPs

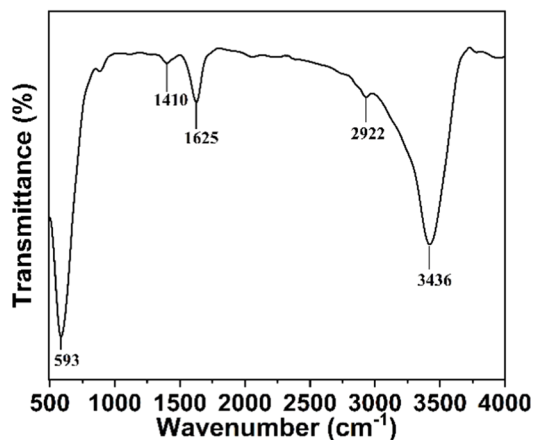

(b) Agar before and after pretreatment

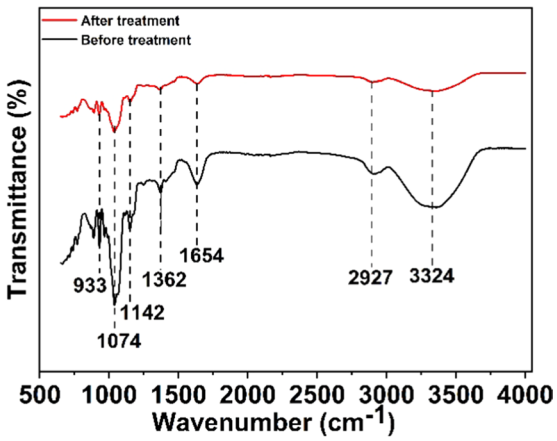

Fig. 8 FTIR analysis of; (**a**) synthesized Fe_3O_4-MNPs, and (**b**) agar before and after pretreatment

Catalytic hydrolysis of agar for reducing sugar production

For the production of the reducing sugars from agar, 1% of agar was hydrolyzed with the synthesized Fe_3O_4-MPNs in 250 mL of a flask and incubated at 30°C while shaking at 200 rpm. For enhancing the production of the reducing sugars, different concentrations of Fe_3O_4-MPNs (0.1–1%) at various temperatures (30–60 °C) with different mixture solutions were monitored (dH_2O, $dH_2O + H_2O_2$, only H_2O_2, 0.1 M

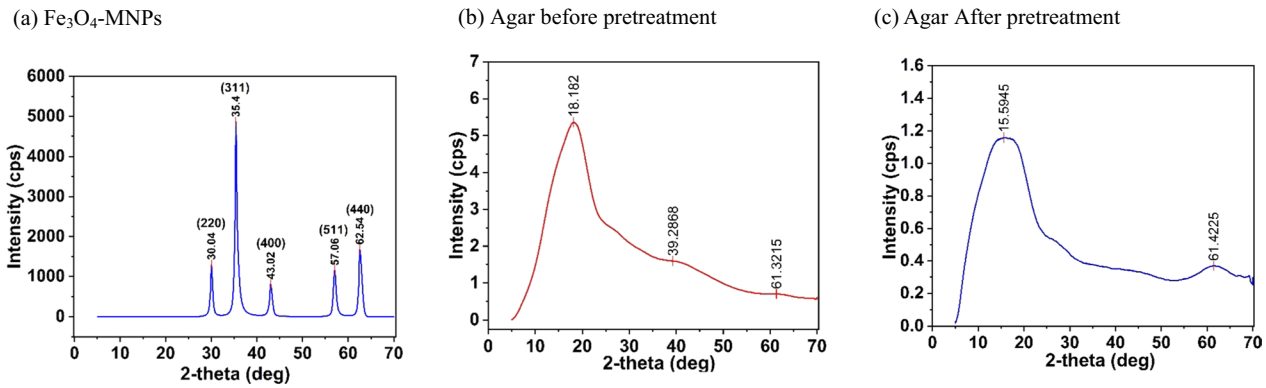

Fig. 9 XRD characterization of; (**a**) synthesized Fe_3O_4-MNPs, (**b**) agar before pretreatment, and (**c**) agar after pretreatment

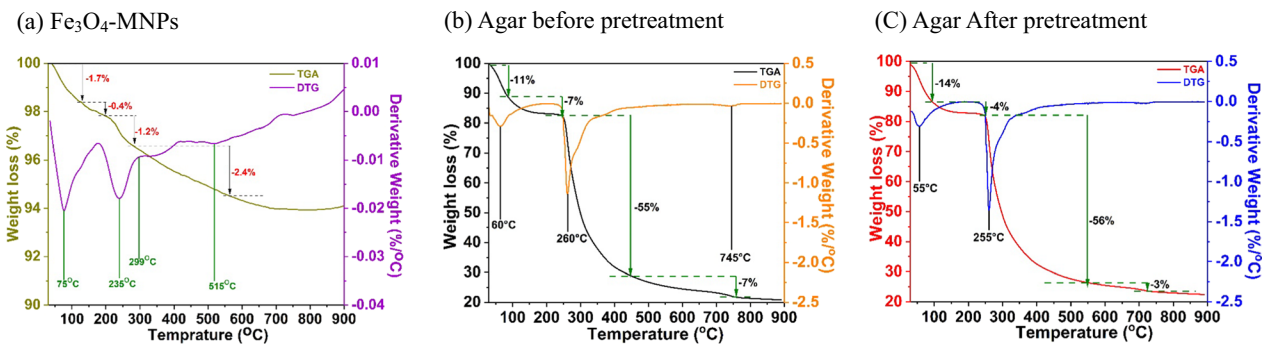

Fig. 10 TGA and DTG characterization of (**a**) synthesized Fe_3O_4-MNPs, (**b**) agar before pretreatment, and (**c**) agar after pretreatment

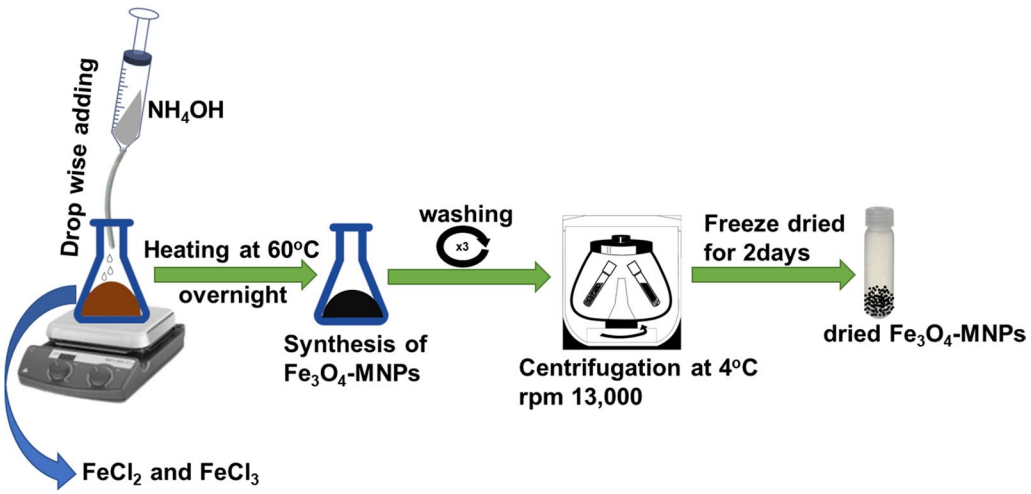

Fig. 11 Schematic diagram of the chemically synthesis of magnetic iron nanoparticle (Fe_3O_4MNPs)

and 0.5 M citrate buffer with varying concentrations (100–500 mg/L) of H_2O_2). After hydrolysis, the solution was recovered by centrifugation at 13,000 rpm for 30 min at 4 °C, and the release of the reducing sugar was measured using the 3,5-dinitrosalicylic acid (DNS) (Sigma-Aldrich) method [61].

Optimization and experimental design

A central composite design (CCD) with independent variables was applied to optimize the significant parameters for the production of bioethanol using the RSM [Design Expert (version 13)]. To determine the individual and interaction effects associated with the process parameters, a CCD factorial design was employed [62, 63]. For error reduction and the uncontrolled factor effects on the response variables, the experimental response was randomized. Following the experimental design, the range and level factors were altered. The response prediction of the correlation and independent variables is illustrated in Eq. 3 as follows:

$$Y = f(X1, X2, X3 \ldots\ldots\ldots\ldots \mathrm{Xn}) + \varepsilon \quad (3)$$

where Y represents the response, X_1 to X_n indicates the independent variables, and 'ε' denotes an experimental error. The actual values of the factors and their corresponding coded levels are listed in Table 6. Likewise, $-\alpha, -1, 0, +1$, and $+\alpha$ indicate five coded levels and their respective values. Using CCD, three different variables (X_1: hydrolysate, X_2: temperature, and X_3: time) were created to develop the experimental runs. To determine the tentative bioethanol concentration, separate experiments were conducted depending on the response variables (Table 1). Based on Table 6, the effects of the different hydrolysate concentrations (1.48%, 10%, 22.5%, 35%, and 43.52%) on the production of bioethanol were estimated. In addition, various temperatures [27.61, 30, 35.5, 37, and 39.39 °C for *Escherichia coli* K12 and 26.59, 30, 35, 40, and 43.41 °C for *Saccharomyces cerevisiae* S288c (ATCC 7754)] and times (1.3, 3, 5.5, 8, and 9.07 h) were evaluated to determine the optimum bioethanol production. The analysis of variance (ANOVA) was used to estimate the significance of each factor in the model. Linear, quadratic, and interaction coefficient analyses in terms of the F and p values are shown in Table 2, demonstrating the significance of the individual and correlated process parameter effects through the response variables. The interaction effect of the two independent variables on the production of bioethanol was visualized using a 3D surface plot.

Statistical analysis and model fitting

RSM optimization can be categorized into three major phases: statistical design of experiments, evaluation of coefficients in mathematical models, and validation of the model design [62, 63]. The following equation indicates the calculation of the coded values of the variables from the actual values of the variables:

$$Xi = \frac{Xi - Xo}{\Delta \mathrm{Xi}} \quad (4)$$

where $i = 1,2,3\ldots\ldots$, and Xi denotes the variable-coded values X_i; X_i and X_0 represent the actual independent variable values at the center point, and ΔXi represents the increment [64].

Individual experiments were conducted for each experimental run to obtain the potential of the bioethanol production, as illustrated in Table 1a, b. To calculate the coefficients for both the individual and combined impacts of the factors, the experimental data were fitted to the following quadratic model:

$$Y = \beta_0 + \sum_{i=1}^{n} \beta iXi + \sum_{i=1}^{n} \beta iixi^2 + \sum_{i<j}^{n} \sum_{j}^{n} \beta ijXiXj + \varepsilon \quad (5)$$

Here, Y denotes the measured response variable (percentage of bioethanol production), n is the number of independent variables, X_i and X_j represent the coded independent variables, and β_0, β_i, β_{ii}, β_{ij} are the regression constant, linear coefficient, quadratic coefficient, and interaction coefficient, respectively. ε represents the random error estimated from the difference in the observed and experimental values [65].

Table 6 Experimental range and levels used in central composite design matrix for ethanol production

Independent variables	Range and level					
	Symbol	$-\alpha$	−1	0	1	$+\alpha$
(a) *Escherichia coli* K12						
Hydrolysate concentration (%)	X_1	1.48	10.00	22.5	35.00	43.52
Temperature (°C)	X_2	27.61	30.00	33.50	37.00	39.39
Time (H)	X_3	1.30	3.00	5.50	8.00	9.07
(b) *Saccharomyces cerevisiae* S288c (ATCC 7754)						
Hydrolysate concentration (%)	X_1	1.48	10.00	22.5	35.00	43.52
Temperature (°C)	X_2	26.59	30.00	35.0	40.00	43.41
Time (H)	X_3	1.30	3.00	5.50	8.00	9.07

Saccharification and fermentation of pretreatment agar

The saccharification of agar hydrolysis was micro-aerobically conducted using *Saccharomyces cerevisiae* S288c (ATCC 7754) and *Escherichia coli* K12 in 100 mL of YM and LB broths containing different concentrations of pretreatment agar solution, respectively. After an equal interval of time, a 1 mL reaction sample was aliquoted to estimate the concentration of bioethanol.

Analytical methods

The bioethanol concentration was measured using an ethanol assay kit (PicoSens™ Ethanol Assay Kit (Colorimetric), Biomax) following the manufacturing company. After centrifugation, the reaction solution was diluted 1:1 with 1X PBS buffer (NaCl, KCl, Na_2HPO_4, and KH_2PO_4, pH 7.4). An equal volume of ethanol assay mixture (a mixture of NAD, ethanol probe, enzyme mix, and assay buffer) was added to each well and incubated for 30 min at room temperature. Stop solution was then added to each well, and the absorbance was measured at a wavelength of 450 nm. The bioethanol concentration was calculated by correlating it with the ethanol standard curve (Fig. 12). All experiments were performed in triplicate.

Model validation

For model validation, the predicted optimum values of the different parameters from the CCD were employed in independent experiments. The experiments were performed at least three times to ensure the reproducibility of the results.

Characterization of nanoparticles and agar

Fe_3O_4-MNPs and agar were characterized using different techniques, such as FTIR spectroscopy (Agilent Technologies (Cary 610/660), XRD [Bruker (D2 Phaser)], SEM (HITACHI (SU3800), TEM (JEM-2100 F HR, Jeol LTD), EDS [JEOL (JSM-6700F/JEOL)], and TGA [TA (SDT 650)].

FTIR was used to determine the major functional groups [66]. The sample was finely ground by mixing it with KBr at a ratio of 1:100 and subsequently pressed to form a thin layer of transparent pellets. Observations were recorded in the range of 4000–5000 cm^2. Similarly, XRD was conducted to characterize the crystallinity of the synthesized Fe_3O_4-MNPs and agar applying the following conditions: cu-Kα radiation (λ = 1.540593 A°) in the 2θ range of 5–70° with a stepwise change of 0.0200°. A specific voltage of 45 kV and current of 200 mA were fixed during the analysis. SEM and EDS were used to characterize the surface morphology of the synthesized Fe_3O_4-MNPs and agar [67]. Thermogravimetric profiles of the synthesized Fe_3O_4-MNPs and agar before and after treatment were determined using TGA. Nearly 10 mg of sample was placed inside the TGA instrument, and the weight loss was constantly measured as the temperature increased from 30 to 900 °C at a controlled heating rate of 10 °C/min under an inert environment (nitrogen gas) without oxygen [57].

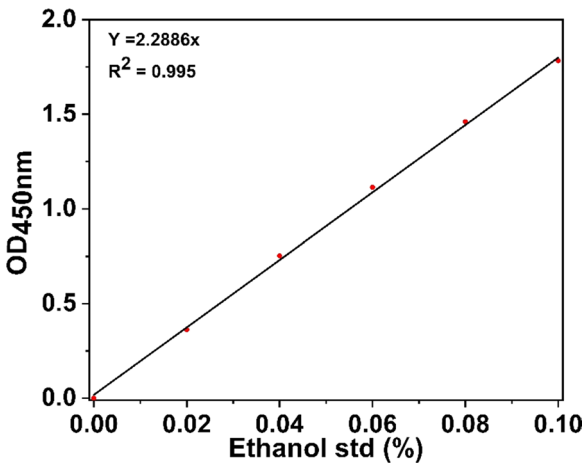

Fig. 12 Ethanol standard curve

Conclusion

This study emphasizes the future prospects of utilizing abundantly available renewable algal biomass for bioethanol production. The use of the synthesized Fe_3O_4-MNPs for agar hydrolysis is faster, simpler, and more economical considering NP application. Furthermore, process optimization using RSM was conducted for comparative bioethanol production, where the agar hydrolysate formed after NP-treated agar demonstrated a significant efficiency in agar degradation. The studies reported thus far have employed simultaneous saccharification using enzymatic hydrolysis and demonstrated a relatively higher ethanol production; however, certain unsolved aspects remain to be addressed. In contrast, the ethanol yield achieved in this study was comparatively lower than those reported, but can overcome the drawbacks of the several other pretreatment methods. In summary, NP-treated agar hydrolysis can be commercialized as a novel method for ethanol production, for which further strategies can be applied to enhance the production rate.

Author contributions

AM: conceptualization, methodology, formal analysis, investigation, and writing of the original draft. WHC: graphical analysis. HTK reviewed and edited the manuscript. JHP supervised, reviewed, edited, and wrote the final draft.

Funding
This research was supported by a National Research Foundation of Korea (NRF) grant funded by the Ministry of Science and ICT (MSIT) (NRF-2020R1C1C1005719 and 2022R1A4A1033015), the R&D program of KEIT (20025698), and the Korea Research Institute of Bioscience and Biotechnology (KRIBB) Research Initiative Program (KGM5362322).

Availability of data and materials
Available on request.

Declarations

Ethics approval and consent to participate
This article does not contain any studies with human participants or animals performed by any of the authors.

Consent for publication
All authors agreed to submit this manuscript.

Competing interests
None.

Received: 13 October 2023 Accepted: 27 November 2023
Published online: 13 December 2023

References

1. Von Hofsten B, Malmqvist M. Degradation of agar by a gram negative bacterium. J Gen Microbiol. 1975;87:150–8.
2. Knutsen SH, Myslabodski DE, Larsen B, Usov AI. A modified system of nomenclature for red algal galactans. Bot Mar. 1994;37:163–70.
3. Park SH, Lee CR, Hong SK. Implications of agar and agarase in industrial applications of sustainable marine biomass. Appl Microbiol Biotechnol. 2020;104:2815–32.
4. Duckworth M, Yaphe W. The structure of agar: Part I Fractionation of a complex mixture of polysaccharides | Semantic Scholar. Carbohydr Res. 1971;16(1):189–97.
5. Kwon M, Jang WY, Kim GM, Kim YH. Characterization and application of a recombinant exolytic GH50A β-agarase from *Cellvibrio* sp. KY-GH-1 for enzymatic production of neoagarobiose from agarose. ACS Omega. 2020;5:29453–64.
6. Chi WJ, Park JS, Kwak MJ, Kim JF, Chang YK, Hong SK. Isolation and characterization of a novel agar-degrading marine bacterium, *Gayadomonas joobiniege* gen, nov, sp. nov, from the Southern Sea Korea. J Microbiol Biotechnol. 2013;23:1509–18.
7. Chen X, Fu X, Huang L, Xu J, Gao X. Agar oligosaccharides: a review of preparation, structures, bioactivities and application. Carbohyd Polym. 2021;256: 118076.
8. Chi WJ, Chang YK, Hong SK. Agar degradation by microorganisms and agar-degrading enzymes. Appl Microbiol Biotechnol. 2012;94:917–30.
9. Ingle AP, Philippini RR, Rai M, Da Silva SS. Catalytic hydrolysis of cellobiose using different acid-functionalised Fe_3O_4 magnetic nanoparticles. IET Nanobiotechnol. 2020;14:40–6.
10. Lai DM, Deng L, Li J, Liao B, Guo QX, Fu Y. Hydrolysis of cellulose into glucose by magnetic solid acid. Chemsuschem. 2011;4:55–8.
11. Ji R, Liu M, Zhang J, Hu Z, Zheng H, Hou Y, et al. Regulation of oxygen-containing functional groups of dual acid core-shell carbon-based catalysts and induction of xylose hydrothermal conversion. Ind Crops Prod. 2023;206: 117708.
12. Guessous G, Patsalo V, Balakrishnan R, Caglar T, Williamson JR, Hwa T. Inherited chitinases enable sustained growth and rapid dispersal of bacteria from chitin particles. Nat Microbiol. 2023;8:1695–705.
13. Thukral M, Allen AE, Petras D. Progress and challenges in exploring aquatic microbial communities using non-targeted metabolomics. ISME J. 2023;17:1–13.
14. Rana MS, Prajapati SK. Microwave-assisted pretreatment of wet microalgal biomass for recovery of biofuel precursors. Fuel. 2021;305: 121610.
15. Pan Y, Alam MA, Wang Z, Huang D, Hu K, Chen H, et al. One-step production of biodiesel from wet and unbroken microalgae biomass using deep eutectic solvent. Bioresour Technol. 2017;238:157–63.
16. Tommasi E, Cravotto G, Galletti P, Grillo G, Mazzotti M, Sacchetti G, et al. Enhanced and selective lipid extraction from the microalga *P. tricornutum* by dimethyl carbonate and supercritical CO2 using deep eutectic solvents and microwaves as pretreatment. ACS Sustain Chem Eng. 2017;5:8316–22.
17. Guisnet M, Pinard L. Characterization of acid-base catalysts through model reactions. Catal Rev Sci Eng. 2018;60:337–436.
18. Gao B, Li L, Wu H, Zhu D, Jin M, Qu W, et al. A novel strategy for efficient agaro-oligosaccharide production based on the enzymatic degradation of crude agarose in *Flammeovirga pacifica* WPAGA1. Front Microbiol. 2019;10: 461293.
19. Kumar AK, Sharma S. Recent updates on different methods of pretreatment of lignocellulosic feedstocks: a review. Bioresour Bioprocess. 2017;4:1–9.
20. Lee HR, Kazlauskas RJ, Park TH. One-step pretreatment of yellow poplar biomass using peracetic acid to enhance enzymatic digestibility. Sci Rep. 2017;7:12216.
21. Liu W, Chen W, Hou Q, Wang S, Liu F. Effects of combined pretreatment of dilute acid pre-extraction and chemical-assisted mechanical refining on enzymatic hydrolysis of lignocellulosic biomass. RSC Adv. 2018;8:10207–14.
22. Rao J, Lv Z, Chen G, Peng F. Hemicellulose: structure, chemical modification, and application. Prog Polym Sci. 2023;140: 101675.
23. Saadattalab V, Jansson K, Tai CW, Hedin N. Blue hydrochars formed on hydrothermal carbonization of glucose using an iron catalyst. Carbon Trends. 2022;8: 100172.
24. Paajanen A, Vaari J. High-temperature decomposition of the cellulose molecule: a stochastic molecular dynamics study. Cellulose. 2017;24:2713.
25. Sherpa KC, Ghangrekar MM, Banerjee R. A green and sustainable approach on statistical optimization of laccase mediated delignification of sugarcane tops for enhanced saccharification. J Environ Manage. 2018;217:700–9.
26. Lyu H, Zhang J, Zhou J, Shi X, Lv C, Geng Z. A subcritical pretreatment improved by self-produced organic acids to increase xylose yield. Fuel Process Technol. 2019;195: 106148.
27. Singhvi M, Kim BS. Green hydrogen production through consolidated bioprocessing of lignocellulosic biomass using nanobiotechnology approach. Bioresour Technol. 2022;365: 128108.
28. Karim MN, Anderson SR, Singh S, Ramanathan R, Bansal V. Nanostructured silver fabric as a free-standing NanoZyme for colorimetric detection of glucose in urine. Biosens Bioelectron. 2018;110:8–15.
29. Singh S. Nanomaterials exhibiting enzyme-like properties (Nanozymes): Current advances and future perspectives. Front Chem. 2019;7: 438937.
30. Wang D, Ikenberry M, Peña L, Hohn KL, Wang D, Ikenberry M, et al. Acid-functionalized nanoparticles for pretreatment of wheat straw. J Biomater Nanobiotechnol. 2012;3:342–52.
31. Laurens LML, Nagle N, Davis R, Sweeney N, Van Wychen S, Lowell A, et al. Acid-catalyzed algal biomass pretreatment for integrated lipid and carbohydrate-based biofuels production. Green Chem. 2015;17:1145.
32. Koo H, Salunke BK, Iskandarani B, Oh WG, Kim BS. Improved degradation of lignocellulosic biomass pretreated by Fenton-like reaction using Fe_3O_4 magnetic nanoparticles. Biotechnol Bioprocess Eng. 2017;22:597–603.
33. Lin Y, Zhang W, Li C, Sakakibara K, Tanaka S, Kong H. Factors affecting ethanol fermentation using *Saccharomyces cerevisiae* BY4742. Biomass Bioenerg. 2012;47:395–401.
34. Kim JH, Ryu J, Huh IY, Hong SK, Kang HA, Chang YK. Ethanol production from galactose by a newly isolated *Saccharomyces cerevisiae* KL17. Bioprocess Biosyst Eng. 2014;37:1871–8.
35. Gupta A, Verma JP. Sustainable bio-ethanol production from agro-residues: a review. Renew Sustain Energy Rev. 2015;41:550–67.
36. Dos Santos LV, De Barros Grassi MC, Gallardo JCM, Pirolla RAS, Calderón LL, De Carvalho-Netto OV, et al. Second-generation ethanol: the need is becoming a reality. Ind Biotechnol. 2016;12:40–57.

37. Offei F, Mensah M, Thygesen A, Kemausuor F. Seaweed bioethanol production: a process selection review on hydrolysis and fermentation. Fermentation. 2018;4:99.
38. Kamzon MA, Abderafi S, Bounahmidi T. Promising bioethanol processes for developing a biorefinery in the Moroccan sugar industry. Int J Hydrogen Energy. 2016;41:20880–96.
39. Branco RHR, Serafim LS, Xavier AMRB. Second generation bioethanol production: on the use of pulp and paper industry wastes as feedstock. Ferment. 2018;5:4.
40. Kubicek CP, Kubicek EM. Enzymatic deconstruction of plant biomass by fungal enzymes. Curr Opin Chem Biol. 2016;35:51–7.
41. Moreira LRS, Filho EXF. Insights into the mechanism of enzymatic hydrolysis of xylan. Appl Microbiol Biotechnol. 2016;100:5205–14.
42. Volynets B, Ein-Mozaffari F, Dahman Y. Biomass processing into ethanol: Pretreatment, enzymatic hydrolysis, fermentation, rheology, and mixing. Green Process Synth. 2017;6:1–22.
43. Korany MA, Fahmy OT, Mahgoub H, Maher HM. High performance liquid chromatographic determination of some guaiphenesin-containing cough-cold preparations. J Adv Res. 2011;2:121–30.
44. Zhang T, Wang L, He X, Lu H, Gao L. Cytocompatibility of pH-sensitive, chitosan-coated Fe_3O_4 nanoparticles in gynecological cells. Front Med. 2022;9: 799145.
45. Bertolucci E, Galletti AMR, Antonetti C, Marracci M, Tellini B, Piccinelli F, et al. Chemical and magnetic properties characterization of magnetic nanoparticles. Conf Rec IEEE Instrum Meas Technol Conf. 2015;2015:1492–6.
46. Rezazadeh L, Sharafi S, Schaffie M, Ranjbar M. Synthesis and characterization of magnetic nanoparticles from raffinate of industrial copper solvent extraction plants. Mater Chem Phys. 2019;229:372–9.
47. Mahdavi M, Bin AM, Haron MJ, Namvar F, Nadi B, Ab Rahman MZ, et al. Synthesis, surface modification and characterisation of biocompatible magnetic iron oxide nanoparticles for biomedical applications. Molecules. 2013;18:7533–48.
48. Mokhtar A, Abdelkrim S, Sardi A, Benyoub A, Besnaci H, Cherrak R, et al. Preparation and characterization of anionic composite hydrogel for dyes adsorption and filtration: non-linear isotherm and kinetics modeling. J Polym Environ. 2020;28:1710–23.
49. Abas SNA, Ismail MHS, Siajam SI, Kamal ML. Comparative study on adsorption of Pb(II) ions by alginate beads and mangrove-alginate composite beads. Adv Mater Res. 2015;1113:248–54.
50. Lyons JG, Geever LM, Nugent MJD, Kennedy JE, Higginbotham CL. Development and characterisation of an agar-polyvinyl alcohol blend hydrogel. J Mech Behav Biomed Mater. 2009;2:485–93.
51. El-Hefian EA, Nasef MM, Yahaya AH. Preparation and characterization of chitosan/agar blended films: part 1 chemical structure and morphology. E-J Chem. 2012;9:1431–9.
52. Setyaningrum DL, Riyanto S, Rohman A. Analysis of corn and soybean oils in red fruit oil using FTIR spectroscopy in combination with partial least square. Int Food Res J. 2013;20:1977–81.
53. Mecozzi M, Pietroletti M, Scarpiniti M, Acquistucci R, Conti ME. Monitoring of marine mucilage formation in Italian seas investigated by infrared spectroscopy and independent component analysis. Environ Monit Assess. 2012;184:6025–36.
54. Raman M, Devi V, Doble M. Biocompatible I-carrageenan-γ-maghemite nanocomposite for biomedical applications-synthesis, characterization and in vitro anticancer efficacy. J Nanobiotechnology. 2015;13:1–13.
55. Wahlström N, Harrysson H, Undeland I, Edlund U. Erratum: a strategy for the sequential recovery of biomacromolecules from red macroalgae *Porphyra umbilicalis* Kützing. Indust Eng Chem Res. 2018;57:42–53.
56. Xu J, Ju C, Sheng J, Wang F, Zhang Q, Sun G, et al. Synthesis and characterization of magnetic nanoparticles and its application in lipase immobilization. Bull Korean Chem Soc. 2013;34:2408–12.
57. Maharjan A, Dikshit PK, Gupta A, Kim BS. Catalytic activity of magnetic iron oxide nanoparticles for hydrogen peroxide decomposition: optimization and characterization. J Chem Technol Biotechnol. 2020;95:2495–508.
58. Gautam R, Varma AK, Vinu R. Apparent kinetics of fast pyrolysis of four different microalgae and product analyses using pyrolysis-FTIR and pyrolysis-GC/MS. Energy Fuels. 2017;31:12339–49.
59. Miranda MT, Sepúlveda FJ, Arranz JI, Montero I, Rojas CV. Physical-energy characterization of microalgae *Scenedesmus* and experimental pellets. Fuel. 2018;226:121–6.
60. Gai C, Liu Z, Han G, Peng N, Fan A. Combustion behavior and kinetics of low-lipid microalgae via thermogravimetric analysis. Bioresour Technol. 2015;181:148–54.
61. Jain A, Jain R, Jain S. Quantitative analysis of reducing sugars by 3, 5-dinitrosalicylic acid (DNSA Method). Basic Techniq Biochem Microbio Mol Bio Prin Techniq. 2020;2020:181–3.
62. Behera SK, Meena H, Chakraborty S, Meikap BC. Application of response surface methodology (RSM) for optimization of leaching parameters for ash reduction from low-grade coal. Int J Min Sci Technol. 2018;28:621–9.
63. Bajpai S, Gupta SK, Dey A, Jha MK, Bajpai V, Joshi S, et al. Application of central composite design approach for removal of chromium (VI) from aqueous solution using weakly anionic resin: modeling, optimization, and study of interactive variables. J Hazard Mater. 2012;227–228:436–44.
64. Ahmadi M, Rahmani K, Rahmani A, Rahmani H. Removal of benzotriazole by Photo-Fenton like process using nano zero-valent iron: response surface methodology with a Box-Behnken design. Polish J Chem Technol. 2017;19:104–12.
65. Rastkari N, Eslami A, Nasseri S, Piroti E, Asadi A. Optimizing parameters on NanophotocatalyticDegradation of Ibuprofen using UVC/ZnOProcesses by response surface methodology. Polish J Environ Stud. 2017;26:785–94.
66. Lesiak B, Rangam N, Jiricek P, Gordeev I, Tóth J, Kövér L, et al. Surface study of Fe_3O_4 nanoparticles functionalized with biocompatible adsorbed molecules. Front Chem. 2019;7:642.
67. Adel Naji A, Tark Abd Ali Z. A single-step method as a green approach to fabricate magnetite nanocomposite for removal of moxifloxacin and cadmium from aqueous solutions. Environ Nanotechnol Monit Manag. 2023;20:100883.
68. Trivedi N, Reddy CRK, Radulovich R, Jha B. Solid state fermentation (SSF)-derived cellulase for saccharification of the green seaweed *Ulva* for bioethanol production. Algal Res. 2015;9:48–54.
69. Trivedi N, Gupta V, Reddy CRK, Jha B. Enzymatic hydrolysis and production of bioethanol from common macrophytic green alga *Ulva fasciata* Delile. Bioresour Technol. 2013;150:106–12.
70. Wu FC, Wu JY, Liao YJ, Wang MY, Shih IL. Sequential acid and enzymatic hydrolysis in situ and bioethanol production from *Gracilaria* biomass. Bioresour Technol. 2014;156:123–31.
71. Park JH, Hong JY, Jang HC, Oh SG, Kim SH, Yoon JJ, et al. Use of *Gelidium amansii* as a promising resource for bioethanol: a practical approach for continuous dilute-acid hydrolysis and fermentation. Bioresour Technol. 2012;108:83–8.
72. Kim NJ, Li H, Jung K, Chang HN, Lee PC. Ethanol production from marine algal hydrolysates using *Escherichia coli* KO11. Bioresour Technol. 2011;102:7466–9.
73. Tan IS, Lam MK, Lee KT. Hydrolysis of macroalgae using heterogeneous catalyst for bioethanol production. Carbohydr Polym. 2013;94:561–6.
74. Lee SM, Lee JH. Ethanol fermentation for main sugar components of brown-algae using various yeasts. J Ind Eng Chem. 2012;18:16–8.
75. Monrroy M, García JR, Mendonça RT, Baeza J, Freer J. Kraft pulping of *Eucalyptus globulus* as a pretreatment for bioethanol production by simultaneous saccharification and fermentation. J Chil Chem Soc. 2012;57:1113–7.
76. Amoah J, Ishizue N, Ishizaki M, Yasuda M, Takahashi K, Ninomiya K, et al. Development and evaluation of consolidated bioprocessing yeast for ethanol production from ionic liquid-pretreated bagasse. Bioresour Technol. 2017;245:1413–20.
77. Kim M, Singhvi MS, Kim BS. Eco-friendly and rapid one-step fermentable sugar production from raw lignocellulosic biomass using enzyme mimicking nanomaterials: a novel cost-effective approach to biofuel production. Chem Eng J. 2023;465: 142879.
78. Schroeder BG, Zanoni PRS, Magalhães WLE, Hansel FA, Tavares LBB. Evaluation of biotechnological processes to obtain ethanol from recycled paper sludge. J Mater Cycles Waste Manag. 2017;19:463–72.
79. Ko CH, Wang YN, Chang FC, Chen JJ, Chen WH, Hwang WS. Potentials of lignocellulosic bioethanols produced from hardwood in Taiwan. Energy. 2012;44:329–34.
80. Nieves IU, Geddes CC, Mullinnix MT, Hoffman RW, Tong Z, Castro E, et al. Injection of air into the headspace improves fermentation of phosphoric acid pretreated sugarcane bagasse by *Escherichia coli* MM170. Bioresour Technol. 2011;102:6959–65.

81. Lan TQ, Gleisner R, Zhu JY, Dien BS, Hector RE. High titer ethanol production from SPORL-pretreated lodgepole pine by simultaneous enzymatic saccharification and combined fermentation. Bioresour Technol. 2013;127:291–7.
82. Mohsenzadeh A, Jeihanipour A, Karimi K, Taherzadeh MJ. Alkaline pretreatment of spruce and birch to improve bioethanol and biogas production. BioResources. 2012;87:1209–14.
83. Li HQ, Li CL, Sang T, Xu J. Pretreatment on *Miscanthus lutarioriparious* by liquid hot water for efficient ethanol production. Biotechnol Biofuels. 2013;6:1.

Publisher's Note